GEOCHRONOMETRIA 53 (2026) 220626
DOI 10.20858/geochr/220626

Available online at https://www.geochronometria.com/

ALIQUOT PREPARATION STRATEGIES AND THEIR IMPACT ON INTER-ALIQUOT REPRODUCIBILITY IN PORTABLE OSL MEASUREMENTS

KEN MUNYIKWA

Centre for Science, Athabasca University, 1 University Drive, Athabasca, Alberta, T9S 3A3, Canada

Received 17 October 2025 Accepted 13 April 2026

Abstract

Over the past decade, the use of portable optically stimulated luminescence (OSL) readers has expanded rapidly, enabling the recovery of latent stratigraphic information from bulk sediments of late Quaternary age. These applications assume that luminescence signals from sample aliquots are reproducible, yet no study has explicitly examined preparation strategies that optimize inter-aliquot consistency. Consequently, no standardized methods for sample preparation exist in portable OSL research. This study initiates this discussion by testing how aliquot preparation and sample size influence reproducibility. Four samples were collected from postglacial eolian dunes in Alberta, Canada. For each sample, 20 aliquots were prepared using four approaches, yielding 320 aliquots: (a) monogranular layers of equal volume portions (~1.5 g), (b) monogranular layers of equal-weight (1.5 g), (c) monogranular layers mounted on double-sided adhesive segments of equal area (~1.0 g), and (d) multilayer portions of equal weight (12.0 g). All aliquots were analyzed with a portable OSL reader. Statistical results showed that for blue-OSL signals, reproducibility varied both among samples and across preparation methods. However, multilayer aliquots prepared with equal weights (12 g) consistently produced the highest reproducibility, suggesting that larger grain populations enhance inter-aliquot consistency. For IRSL signals, no preparation method offered a clear advantage.

Keywords

portable OSL reader; luminescence; aliquots; sample preparation; monogranular layers; multilayer; inter-aliquot consistency; reproducibility

1. Introduction

A growing number of publications has emerged over the last 10–15 years demonstrating the practicality of portable OSL readers in geoscience and archaeological field investigations that examine late Quaternary sequences. The utility of the devices lies in their capacity to rapidly and cost-effectively generate chronological and proxy stratigraphic information about depositional environments, in contrast to relying solely on standard luminescence dating procedures. The devices are lightweight, such that they can be taken to the field or closer to the site. Importantly, sample measurements are much simpler than with standard OSL dating protocols including that no preheating is required. Finally, and most critically, sample measurements using portable OSL readers are commonly performed on unprocessed bulk samples, an aspect that takes a significant amount of time with regular OSL dating where pure quartz or feldspar sand grains (in the coarse-grains method) or fine silt (when using the fine grain approach) are extracted.

The range of studies in which the devices have been used includes contextualization of luminescence characteristics of terrestrial depositional sequences (e.g. Sanderson and Murphy, 2010; Bateman *et al.*, 2015; Portenga and Bishop, 2016; Adolph *et al.*, 2021; Boyd *et al.*, 2022; Schulze *et al.*, 2022; Rex *et al.*, 2022; Robins *et al.*, 2022, 2023; Euzen *et al.*, 2024; Rizza *et al.*, 2024; Roman *et al.*, 2024) and those of archaeologic sedimentary sites (e.g. Srivastava *et al.*, 2023; Sanchez-Pardo *et al.*, 2024;

Corresponding author: K. Munyikwa
e-mail: kenm@athabascau.ca

ISSN 1897-1695 (online), 1733-8387 (print)

Ben-Melech *et al.*, 2024; Robins *et al.*, 2023). In many cases, such studies have been conducted to help screen samples for regular OSL dating. Alternatively, beyond sample screening, portable OSL measurements have also been used to elucidate substratigraphic information that can shed light on paleoenvironmental characteristics at sites that already have well-established chronological records (e.g. Kinnaird *et al.*, 2017; Porat *et al.*, 2019; Rex *et al.*, 2022; Staff *et al.*, 2024). In yet other studies, portable OSL readers have been used to approximate numerical ages of samples by calibrating raw portable OSL reader signals in order to expedite the assignment of a chronology (Munyikwa and Brown, 2014; Stone *et al.*, 2015, 2019, 2024; DuRoss *et al.*, 2022; Nitundil *et al.*, 2023). Luminescence signal characteristics obtained using portable OSL readers have also been used as sediment tracers to establish provenance (e.g. Gray *et al.*, 2022, Muños-Salinas *et al.*, 2023). A comprehensive range of other applications in which portable readers have been used is reviewed in Munyikwa *et al.* (2021).

It should be recognized that portable luminescence signals are affected by several factors, such as burial age, grain sensitivity, dose rate, and the degree of signal resetting before burial (e.g. Sanderson and Murphy, 2010). Sediment grain size and mineral composition also have an influence on the luminescence properties (e.g. Timar-Gabor *et al.*, 2017). Notably, even though the signals yielded by portable OSL readers are proxies for the chronology in a majority of cases, it is not yet possible to use the signals directly to calculate numerical ages. Additionally, because depositional units in their natural setting are rarely homogeneous, the absence of sample processing prior to measurement means that luminescence signals from aliquots of the same sample may be characterized by scatter that is more pronounced than that observed with processed samples. While some mechanisms for normalizing the signals could help in such cases, luminescence intensities from portable OSL measurements are usually not normalized for sensitivity. Normalization that is typically performed for portable OSL measurements is for sample weight (e.g. Rizza *et al.*, 2024). For age estimation, normalization has been performed in some instances using the administration of a post-dose using an external radiation source (e.g. Munyikwa and Brown, 2014).

Luminescence intensity from sample aliquots is the primary variable for characterizing depositional units in portable OSL studies. Whether it is in profiling, which entails analysis of vertical variations in signal intensities down depositional sequences (e.g. Sanderson and Murphy, 2010, Kinnaird *et al.*, 2019; Munyikwa *et al.*, 2021), or in age estimation and using sediment tracers, investigators primarily look at signal intensities as proxies for other characteristics. For any of these studies to be accurate, however, the individual aliquot measurements must be representative. Signal reproducibility or consistency between inter-aliquot measures is a demonstration that measurements are robust and representative. Nonetheless, in routine portable OSL studies, preparing large numbers of aliquots to assess signal consistency for each sample is impractical, as it undermines the rapid analysis that constitutes the main advantage of this approach. One way of ensuring consistency is to systematically employ a measurement protocol that is proven to generate reproducible results.

Although reproducibility of aliquots is essential, descriptions of aliquot preparation and sample mounting in published portable OSL studies have, to date, been sparse. In most cases, authors simply mention that samples were placed in cups and measured using the portable OSL reader. In others, a few additional details are provided. For instance, Adolph *et al.* (2021) explained that around 1–2 grams were placed in 3 cm aluminum cups and the surface of the sediments leveled by compression to create a monolayer. In some studies, multiple aliquots are measured and averages calculated (e.g. Adolph *et al.*, 2021) whereas in others, normalization is performed using weight. The primary objective in most studies, however, appears to be the use of monogranular layers, as these are easier to reproduce and enhance inter-aliquot consistency in surface area.

To initiate a discussion looking into ways of optimizing aliquot preparation techniques for portable OSL measurements, and to assist new users who may be contemplating portable OSL reader studies, this study examines sample mounting methods that can be used with the Scottish Universities Environmental Research Centre (SUERC) portable OSL reader (Sanderson and Murphy, 2010). Four approaches are examined: aliquots with monogranular layers apportioned by volume, aliquots with monogranular layers apportioned by weight, aliquots in which monogranular layers are immobilized using double-sided adhesive tape to eliminate grain movement, and multilayer portions of equal weight. After measurements with a portable OSL reader, data acquired with each method are then analyzed statistically to determine inter-aliquot consistency. Majgier *et al.* (2025) recently reported on the Helios portable OSL reader, which employs a slightly different sample geometry. The present study did not include tests with that system; therefore, all references to the portable OSL reader hereinafter pertain specifically to the SUERC instrument.

2. Materials and methods

2.1. Sampling and sample preparation

To minimize variables that could influence luminescence signal intensities and thereby isolate the effect of aliquot preparation, this study focused on sediments that were well bleached prior to burial. Eolian dune sands were chosen because the subaerial transport that they undergo typically ensures that sediment grains are effectively zeroed of any previously acquired energy at the time of deposition. Accordingly, one sample was collected from each of four postglacial dune fields in central and northern Alberta, Canada: Edson (ED02, 53° 30.238’ N, 116° 36.103’ W; depth 4.6 m), Smith (SM09, 55° 08.781 N, 114° 01.237’ W;

depth 4.3 m), La Crete (LC01, 58° 10.154 N, 114° 01.237 W; depth 4.5 m) and Wood Buffalo (WB01, 59° 26.442' N; 112° 21.023 W; depth 5.5) (**Fig. 1**). The Laurentide Ice Sheet (LIS) covered the region *ca.* 22–20 ka ago during the Last Glacial Maximum (LGM) (Dyke *et al.*, 2002, Dalton *et al.*, 2023). After the LGM, the LIS began to retreat north eastwards starting at *ca.* 17 ka. The drainage of associated glacial lakes left sediments that blanketed former lakebeds, and these deposits were mobilized by wind to form the dune fields. The dune sands in central and northern Alberta have been dated using luminescence methods at about 13–16 ka (Wolfe *et al.*, 2004; Munyikwa *et al.*, 2017).

Before luminescence analysis, each sample was thoroughly mixed to minimize variability in its physical properties. The grain size distribution of each sample was then measured by sieving and grain size parameters calculated using the Gradistat statistical package (Blott and Pye, 2001).

When using the SUERC portable OSL reader as in this study, samples are introduced into the reader for analysis using a 5-cm diameter Petri dish (**Fig. 2**). Using this set up, the evaluation of optimal aliquot preparation strategies necessitates an appreciation of how the OSL reader signal intensities vary with sample aliquot weight, particularly as it pertains to the geometry of the sample aliquot in the Petri dish. As a result, prior to assessing the different aliquot preparation methods, a study was conducted to assess how the signal changed with increasing aliquot weight. Sample WB01 was selected for this analysis and 8 aliquots weighing 0.18, 0.38, 0.75, 1.5, 3.0, 6.0, 12.0, 24.0 g prepared. These were then measured with the portable OSL reader.

To assess the influence of the aliquot preparation strategy on luminescence signal variability, the effects of both the sample apportioning method and the aliquot size were examined. Thus, four preparation methods were employed, as detailed below and summarized in **Table 1**:

- Method 1: 20 aliquots were prepared from each of the four samples by measuring about 1 cm^3 of sediment using a small scoop, ensuring constant volume between each measure. The aliquot from the scoop weighed about 1.5 g. The volume of the sediment created a monogranular layer at the base of the Petri dish that contained the sample. Sample size was controlled by the volume of the scoop; however, weight measurements revealed slight variations between aliquots prepared in this manner.
- Method 2: 20 aliquots were prepared from each sample, with each aliquot consisting of precisely 1.5 g of sediment. Thus, in this instance, aliquot size was controlled by weight. As in Method 1, the sample quantity produced a monogranular layer at the base of the Petri dish.
- Method 3: From each sample, 20 aliquots were prepared by affixing a monogranular layer of sediment to 3.2 × 3.0 cm cardstock segments coated with double-sided adhesive tape. In Methods 1 and 2, the sediment grains were not immobilized; thus, it is possible that some movement occurred during the placement of the Petri dish into the OSL reader. In Method 3, however, such movement could not occur.
- Method 4: 20 aliquots were prepared from each sample by weighing out an aliquot of exactly 12.0 grams into the Petri dish. This amount of sediment filled the Petri dish to a depth of approximately 3.5 mm, producing multiple grain layers.

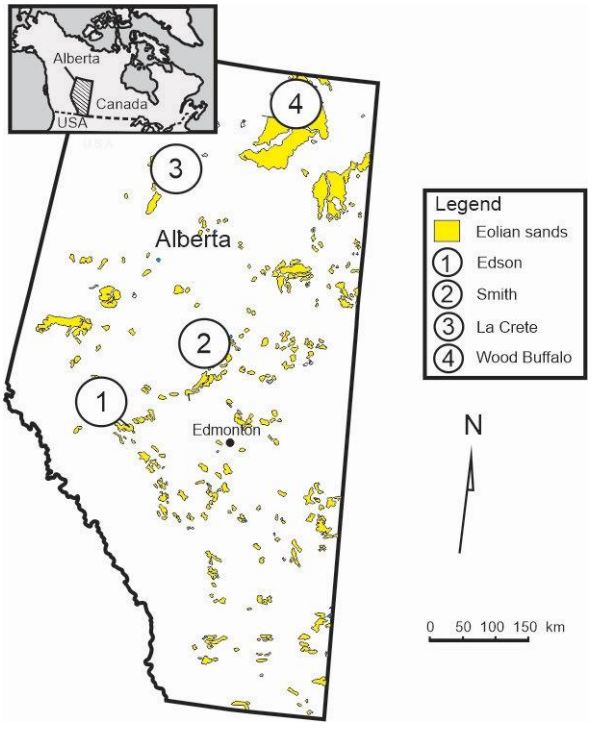

Fig. 1. *Location of sample sites in Alberta, western Canada.*

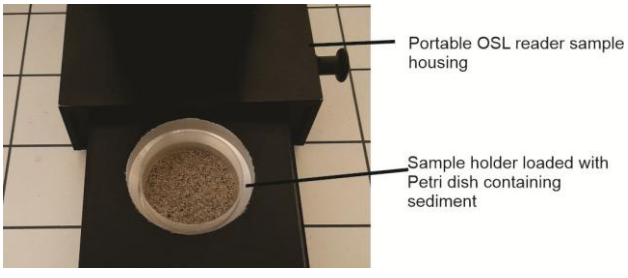

Fig. 2. *Sample mounting tray in a 2nd-generation SUERC portable OSL reader.*

Table 1. *Aliquot preparation methods used in this study.*

Aliquot Preparation Method	Sample and number of aliquots prepared			
	ED02	SM09	LC01	WB01
Method 1: Equal volume monolayer (EV) (~ 1.5 g)	20	20	20	20
Method 2: Equal weight monolayer (EW) (1.5 g)	20	20	20	20
Method 3: Equal area fixed monolayer (EA) (~ 1.0 g)	20	20	20	20
Method 4: Equal weight multigranular layer (ML) (12.0 g)	20	20	20	20

2.2. Portable OSL reader

The SUERC reader is equipped with infrared LEDs whose emission is passed through RG780 long pass filters for a spectrum centred around 880 ± 40 nm as well as blue light LEDs whose emission is filtered through an RG420 long pass filter for an output centred around 470 ± 20 nm. Signals obtained from the sample following stimulation are detected through UG11 filters (Sanderson and Murphy, 2010). For sample measurement, each aliquot was placed in a 3-cm diameter Petri dish before being introduced into the reader (**Fig. 2**). The measurement procedure involved stimulating the samples in continuous-wave mode using infrared-stimulated luminescence (IRSL) for 60 s to target feldspar, followed by a post-IR blue-OSL stimulation targeting quartz. Each measurement cycle sequentially entailed a 15 s dark count, a 60 s IRSL count, a 15 s dark count, a 60 s post-IR blue-OSL count, and a 15 s dark count. The luminescence signal intensity was recorded as total counts.

2.3. Statistical analysis

Luminescence results obtained from the analysis of sample aliquots for evaluating aliquot preparation methods were analyzed using statistical methods. Each set of 20 measurements was first processed with K-means centroid selection, which identified the 10 values closest to the mean. To achieve that, the mean was first calculated, after which the distance of each value from the mean was determined. This enabled the 10 closest values to be selected. To ascertain the degree to which the 10 values were representative of the measured value, the coefficient of variation (CV) was calculated by first determining the mean of the 10 values and their standard deviation after which the following formula was used:

CV= (Standard Deviation / Mean) * 100.

For this study, the CV values were categorized into very high consistency, moderate consistency, low consistency and very low consistency using criteria outlined in **Table 2**.

Table 2. *Classification criteria used to interpret coefficients of variation.*

Coefficient of Variation (CV) %	Classification
< 5.0%	very high consistency, very tightly clustered
5.0–10.0%	moderate consistency
10.0–20.0%	low consistency, variable
> 20.0%	very low consistency, very variable data

2.4. Assessing other variables that may influence aliquot reproducibility

Apart from sample geometry and weight, aliquot signal reproducibility can be influenced by several additional factors, including grain size, mineralogical composition, and overall sample homogeneity. In a study examining the relationship between portable OSL signals and depositional ages of paleowetland sediments, Gray *et al.* (2018) reported that sieving sediments to <250 µm and treating samples with dilute HCl to remove carbonates significantly reduced signal scatter. Removing heavy minerals such as zircon and magnetite using a hand magnet also contributed to the reduction in signal variability. Although zircon, a luminescent mineral, is not inherently magnetic, it can contain microscopic inclusions of iron oxides (e.g. magnetite) that impart magnetic susceptibility, allowing its removal using a magnet (e.g. Fu *et al.*, 2017).

Notwithstanding the above, the sediments analyzed in this study comprise aeolian dune deposits that are generally moderately to well sorted and composed predominantly of quartz, with subordinate feldspar (e.g., Munyikwa *et al.*, 2017). For example, dune sands from southern Alberta have been reported to contain >80% quartz, ~10% feldspar, and ~5% other minerals (Holter, 1971). As such, heavy minerals are unlikely to be a major source of signal scatter in the samples under consideration, leaving feldspar as the only other notable luminescent contributor.

Thus, following luminescence measurements, the potential for inter-aliquot variation in quartz and feldspar content to impact signal reproducibility of IRSL or blue-OSL signals was evaluated using two approaches. First, the depletion index, defined as the ratio of cumulative signal intensity in the first half of the stimulation period to that in the second half (Sanderson and Murphy, 2010), was calculated for each aliquot to assess variability. The depletion index is influenced by variables that include mineralogy and the degree of bleaching prior to burial.

The second approach used to assess variation in feldspar and quartz concentrations between aliquots involved calculating the IRSL/OSL ratio and evaluating inter-aliquot fluctuations. As noted earlier, the IRSL signal is derived from feldspars, whereas the blue-OSL signal is dominated by quartz. Consequently, the IRSL/OSL ratio provides a proxy for variations in feldspar-to-quartz proportions among aliquots (Sanderson and Murphy, 2010). Thus, IRSL/OSL ratios were calculated for each measured aliquot and compared within each sample and across different aliquot preparation methods and sample sites to assess trends.

3. Results

3.1. Change of OSL signal with sample weight

The aliquots prepared to assess the relationship between the aliquot size and signal intensity are shown in **Fig. 3**. Aliquot weights were selected so that the sample initially formed a monogranu lar layer covering only a small fraction of the Petri dish base. As more sediment was added, the layer spread gradually, reaching full coverage of the Petri dish base as a monogranular layer at 1.5 g. From 3.0 g to 24.0 g, the sample's surface area remained constant.

Table 3. *Sample weight vs signal intensity for sample WB01.*

Sample weight (g)	IRSL signal	Blue OSL signal
0.18	142583 ± 378	322882 ± 567
0.38	205432 ± 453	444485 ± 667
0.75	196830 ± 444	471049 ± 687
1.5	207878 ± 457	473876 ± 689
3.0	221329 ± 471	499483 ± 708
6.0	232597 ± 483	533805 ± 731
12.0	245445 ± 992	560867 ± 749
24.0	288001 ± 537	695929 ± 835

However, the aliquot depth increased from approximately 1.0 mm at 3.0 g to about 7.0 mm at 24.0 g. (**Fig. 3**). The results of the experiment to assess signal variation with increasing aliquot size for sample WB01 are listed in **Table 3** and plotted in **Fig. 4**.

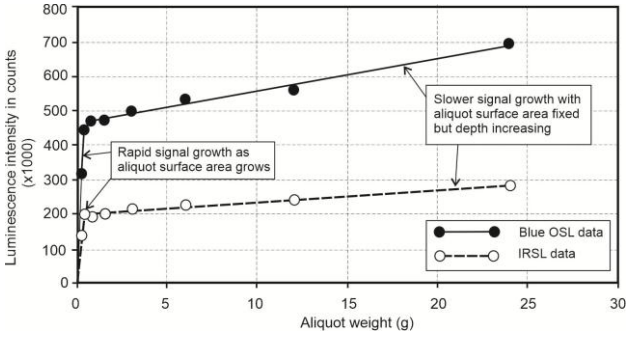

Fig. 4. *IRSL and blue-OSL signal intensities obtained from sample aliquots of increasing weight from 0.18 to 24.0 grams as shown in **Table 3**. The plot displays two regions with clearly different slopes.*

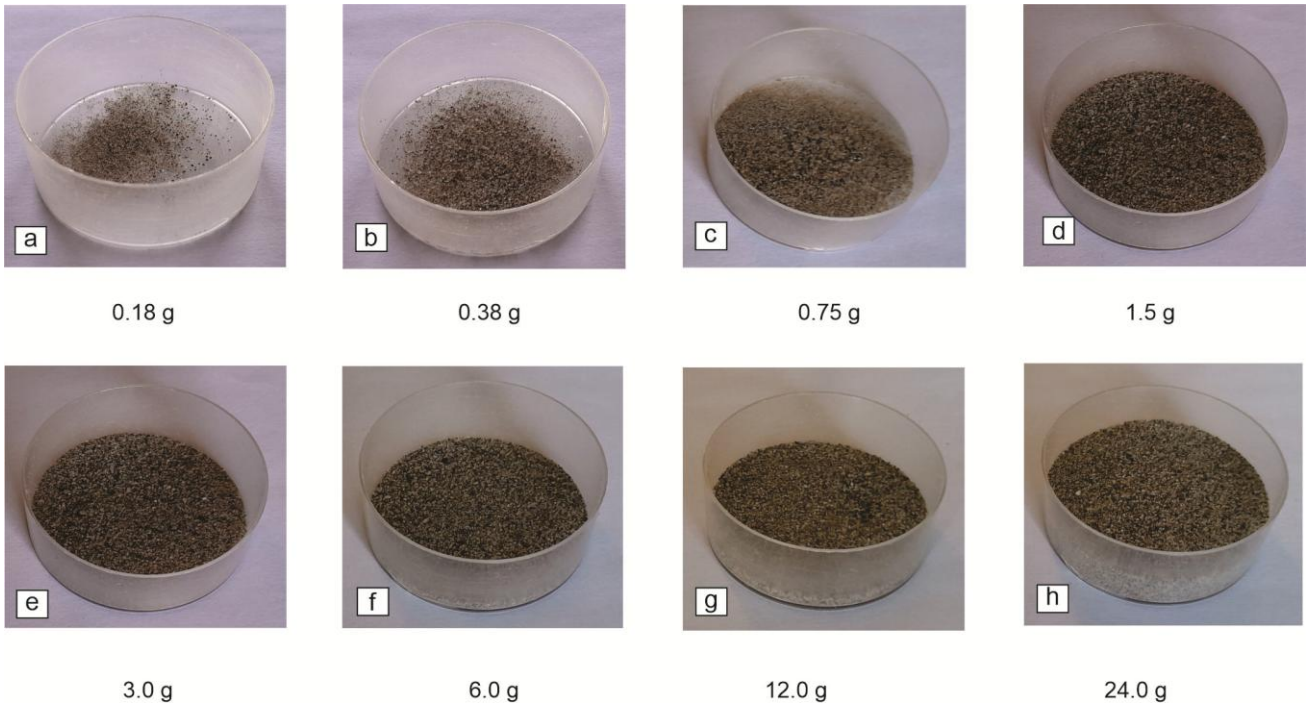

Fig. 3. *Aliquots prepared to evaluate signal intensity variations with aliquot weight. In (a) the sample size is a monogranular layer that covers a small part of the bottom of the petri dish. In (b) and (c) the area covered is larger but not completely. In (d) however, the entire bottom is covered, but the sample is still a monogranular layer. In aliquots (e) to (h), the grains form multilayer samples of increasing depth, ranging from about 1.0 mm in aliquot (e) to 7.0 mm in (h).*

The curves in **Fig. 4** feature two distinct parts for both IRSL and blue-OSL signals. Aliquots of 0.18 and 0.38 g yielded signals that plotted a steep part of the curve, indicating a sharp rise in signal intensity with sample size. From the aliquot weighing 0.75 g, the signal begins to level off for both the IRSL and blue-OSL signals and, from 1.5 g, the curve maintains an approximately constant slope up to 24.0 g. As indicated above, the first two samples (0.18 and 0.38 g) do not cover the bottom of the Petri dish completely. Hence the rapid increase in signal intensity with weight results from the increase in the surface area of the sample exposed to the stimulating source. From aliquot 1.5 g, the base is completely covered such that for any aliquots of greater sample weight, the surface area remains constant. However, the signal intensity continues to rise as aliquot weight increases, despite that the sample surface area remains fixed. This is because the sample depth is increasing, and the optical source of the luminescence reader is able to penetrate the sediment column in the Petri dish.

3.2. Blue-OSL signals from different aliquot preparation methods

A total of 20 aliquots from each of the four samples from sites in **Fig. 1** was prepared using each of the four methods shown in **Fig. 5**. From each set of 20 blue-OSL signal intensities obtained from a given sample, the 10 values closest to the centroid as statistically determined are listed in **Table 4**. IRSL signals for corresponding measurements are also presented. Complete results are provided as supplementary data. Histograms of the 10 blue-OSL values from each set are plotted in **Figs. 6–9**. To facilitate comparison, data from the different sites are organized in **Table 4** and **Figs. 6–9** according to aliquot preparation method. The coefficient of variation calculated for each set of 10 measurements is shown in **Table 5** and **Figs. 6–9**.

For aliquots prepared using equal-volume sediment portions (**Fig. 5a**), three of the samples yielded blue-OSL signals with a CV between 3.8% (LC01) and 4.5% (WB01) (**Fig. 6**) which is an indication that the signals are highly consistent (**Table 2**). One sample (SM09), however, produced aliquots with a CV of 5.9% which is moderately consistent (**Table 2**).

Aliquots prepared using portions of equal weight of 1.5 g (**Fig. 5b**) produced blue-OSL signals that were highly consistent for two of the sites, yielding CVs of 2.2% (LC01) and 2.4% (WB02). The other two samples, however, yielded CVs of 5.2% (SM09) and 6.4% (ED02) which is within the moderately consistent category (**Table 2**).

For the aliquots prepared by mounting about 1.0 g of sediment on double-sided adhesive tape, two of the samples yielded CV values of 3.2% (ED02) and 3.9% (WB01), which is highly consistent (**Table 2**). One sample (LC01) yielded a CV of 5.9% which is moderately consistent. The fourth sample, however (SM09), produced a CV of 11.1% which points to very variable data or low consistency (**Table 2**).

With the fourth and final method whereby portions of equal weight of 12.0 g were prepared, the signals from the aliquots produced CV values of 1.5% (WB01), 3.7% (LC01), 4.1 (SM09) and 3.6% (ED01). These values all fall in the highly reproducible category of tightly clustered data (**Table 2**).

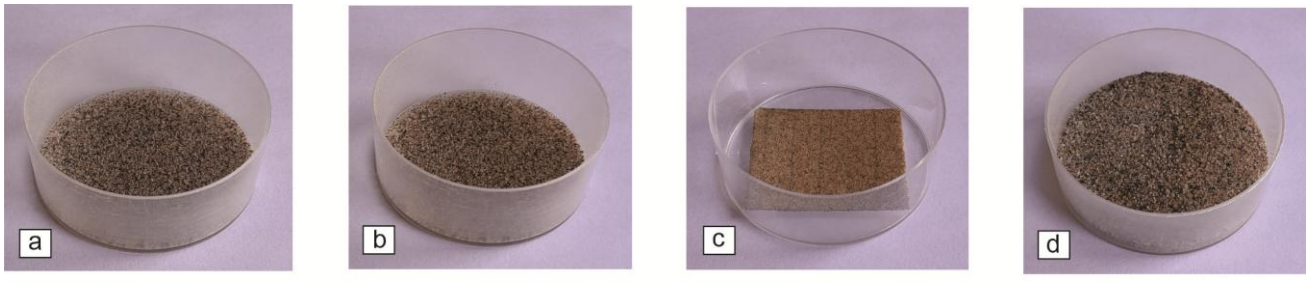

Fig. 5. *Aliquot preparation methods investigated in this study.*

Table 4. *Luminescence results. The 10 IRSL and blue-OSL values closest to the centroid for each data set are shown.*

	ED02-EV		SM09-EV		LC01-EV		WB01-EV	
#	IRSL	Blue-OSL	IRSL	Blue-OSL	IRSL	Blue-OSL	IRSL	Blue-OSL
1	136500 ± 370	301147 ± 549	184150 ± 430	487720 ± 699	216672 ± 446	486164 ± 698	262550 ± 513	562016 ± 750
2	137482 ± 371	318042 ± 564	134992 ± 368	433529 ± 659	210114 ± 459	494607 ± 704	243001 ± 493	498545 ± 706
3	130356 ± 362	288286 ± 537	161371 ± 402	492215 ± 702	201298 ± 449	496274 ± 705	243679 ± 494	548693 ± 741
4	136467 ± 370	304932 ± 553	164671 ± 406	499731 ± 707	209569 ± 458	492722 ± 702	232999 ± 483	524809 ± 725
5	130784 ± 362	280874 ± 530	174687 ± 419	485004 ± 697	228738 ± 479	470613 ± 686	240223 ± 491	513742 ± 717
6	137742 ± 372	309783 ± 557	139738 ± 374	425709 ± 653	207020 ± 456	473590 ± 689	260241 ± 511	570963 ± 756
7	156578 ± 396	305111 ± 553	153108 ± 392	470795 ± 686	224171 ± 574	465625 ± 683	243424 ± 494	544282 ± 738
8	126099 ± 359	317217 ± 564	182931 ± 428	466594 ± 683	196172 ± 443	445672 ± 668	259073 ± 509	563739 ± 751
9	135826 ± 369	305214 ± 553	145110 ± 382	426698 ± 654	202387 ± 450	445382 ± 668	240079 ± 490	563208 ± 751
10	135888 ± 369	315138 ± 562	135956 ± 369	453095 ± 673	195030 ± 442	451854 ± 673	263747 ± 514	572802 ± 757
	ED02-EW		**SM09-EW**		**LC01-EW**		**WB01-EW**	
#	IRSL	Blue-OSL	IRSL	Blue-OSL	IRSL	Blue-OSL	IRSL	Blue-OSL
1	136973 ± 371	294491 ± 543	156682 ± 397	416152 ± 645	230740 ± 481	472984 ± 688	242069 ± 492	532081±730
2	137350 ± 371	296782 ± 545	140536 ± 376	424564 ± 652	216720 ± 466	484312 ± 696	232360 ± 483	504041±710
3	131148 ± 363	291721 ± 541	167775 ± 410	460876 ± 679	205409 ± 454	495778 ± 704	237040 ± 487	514254±717
4	122096 ± 350	254592 ± 505	134360 ± 367	421600 ± 650	200283 ± 448	477075 ± 691	220423 ± 470	498466±706
5	129520 ± 361	274834 ± 525	163058 ± 404	481285 ± 694	212566 ± 462	471871 ± 687	241536 ± 492	516146±719
6	121292 ± 349	254766 ± 505	163504 ± 405	426514 ± 653	207354 ± 456	483719 ± 696	225418 ± 475	497382±706
7	124974 ± 354	268718 ± 519	152630 ± 391	424988 ± 652	204625 ± 453	464604 ± 682	239764 ± 490	529761±671
8	131577 ± 363	272988 ± 523	163051 ± 404	441264 ± 665	210027 ± 459	477189 ± 691	232786 ± 483	499889±683
9	131679 ± 364	305212 ± 553	134370 ± 367	484531 ± 696	197852 ± 445	481533 ± 694	227131 ± 477	520040±738
10	134735 ± 368	287356 ± 537	169572 ± 412	475534 ± 690	193818 ± 441	463287 ± 681	224917 ± 475	506213±712
	ED02-EA		**SM09-EA**		**LC01-EA**		**WB01-EA**	
#	IRSL	Blue-OSL	IRSL	Blue-OSL	IRSL	Blue-OSL	IRSL	Blue-OSL
1	132529 ± 365	261948 ± 512	100152 ± 317	246411 ± 497	139032 ± 374	290236 ± 539	154840 ± 394	294852 ± 543
2	124189 ± 353	249640 ± 500	93100 ± 306	254829 ± 505	147530 ± 385	268307 ± 518	160189 ± 401	314849 ± 546
3	123546 ± 352	240620 ± 491	126546 ± 356	318194 ± 565	137335 ± 371	284690 ± 534	157263 ± 397	300757 ± 549
4	129126 ± 360	244452 ± 495	126045 ± 356	304366 ± 552	133371 ± 366	286528 ± 536	164827 ± 407	334424 ± 579
5	128435 ± 359	249748 ± 500	98943 ± 315	290967 ± 540	135397 ± 369	243310 ± 494	140884 ± 376	294719 ± 543
6	129921 ± 361	245398 ± 496	93391 ± 306	250006 ± 500	133344 ± 366	264210 ± 514	157072 ± 397	313547 ± 560
7	129126 ± 360	253826 ± 504	123725 ± 352	312131 ± 559	120148 ± 347	247561 ± 498	154708 ± 394	324083 ± 570
8	118008 ± 344	236718 ± 487	103602 ± 323	287106 ± 536	131944 ± 364	255664 ± 506	155082 ± 394	331684 ± 576
9	126330 ± 356	246311 ± 497	97450 ± 313	268040 ± 518	129944 ± 361	275575 ± 525	170817 ± 414	316404 ± 563
10	128895 ± 360	264650 ± 515	123093 ± 352	339242 ± 583	126630 ± 357	254161 ± 505	162244 ± 403	313292 ± 560
	ED02-ML		**SM09-ML**		**LC01-ML**		**WB01-ML**	
#	IRSL	Blue-OSL	IRSL	Blue-OSL	IRSL	Blue-OSL	IRSL	Blue-OSL
1	160707 ± 401	319213 ± 565	182558 ± 428	542091 ± 737	219193 ± 469	491268 ± 701	268779 ± 519	601400 ± 776
2	159539 ± 400	348672 ± 591	150338 ± 388	489291 ± 700	250996 ± 501	502170 ± 709	260056 ± 510	606049 ± 779
3	151717 ± 390	326329 ± 572	184957 ± 431	477493 ± 691	217634 ± 467	509517 ± 714	262321 ± 513	623569 ± 790
4	154272 ± 393	329499 ± 567	184821 ± 430	523796 ± 724	219372 ± 469	514990 ± 718	289102 ± 529	622273 ± 689
5	149867 ± 388	328130 ± 573	193894 ± 441	465861 ± 483	213599 ± 463	551413 ± 743	267707 ± 518	614676 ± 784
6	148170 ± 386	308313 ± 556	169177 ± 412	531241 ± 729	223404 ± 473	509023 ± 714	265200 ± 515	609379 ± 781
7	145490 ± 382	319358 ± 566	148327 ± 386	495534 ± 704	200475 ± 448	485018 ± 697	289594 ± 539	617267 ± 786
8	138545 ± 373	312782 ± 560	201393 ± 449	508781 ± 714	230873 ± 481	520555 ± 722	275824 ± 526	605439 ± 778
9	145312 ± 382	315890 ± 562	206106 ± 455	499994 ± 707	208274 ± 457	514404 ± 718	255005 ± 505	591431 ± 769
10	150718 ± 389	307695 ± 555	189698 ± 436	481007 ± 694	197287 ± 445	485679 ± 697	267210 ± 517	615818 ± 785

Table 5. *Coefficients of variation calculated from blue-OSL signals obtained using the different aliquot preparation methods.*

Sample	Equal Volume (monogranular) (EV) (1.5 g) (%)	Equal Weight (monogranular) (EW) (1.5 g) (%)	Equal Area on adhesive tape (monogranular) (EA) (1.0 g) (%)	Equal-Weight Multilayer (ML) (12.0 g) (%)
Edson (ED02)	4.0	6.4	3.2	3.6
Smith (SM09)	5.9	5.2	11.1	4.1
La Crete (LC01)	3.8	2.2	5.9	3.7
Wood Buffalo (WB01)	4.5	2.4	3.9	1.5

Table 6. *Coefficients of variation calculated from IRSL signals obtained using the different aliquot preparation methods.*

Sample	Equal Volume (monogranular) (EV) (1.5 g) (%)	Equal Weight (monogranular) (EW) (1.5 g) (%)	Equal Area on adhesive tape (monogranular) (EA) (1.0 g) (%)	Equal-Weight Multilayer (ML) (12.0 g) (%)
Edson (ED02)	5.9	4.4	3.3	4.5
Smith (SM09)	11.9	8.6	13.3	10.8
La Crete (LC01)	5.4	5.1	5.5	7.1
Wood Buffalo (WB01)	4.5	3.4	4.9	4.3

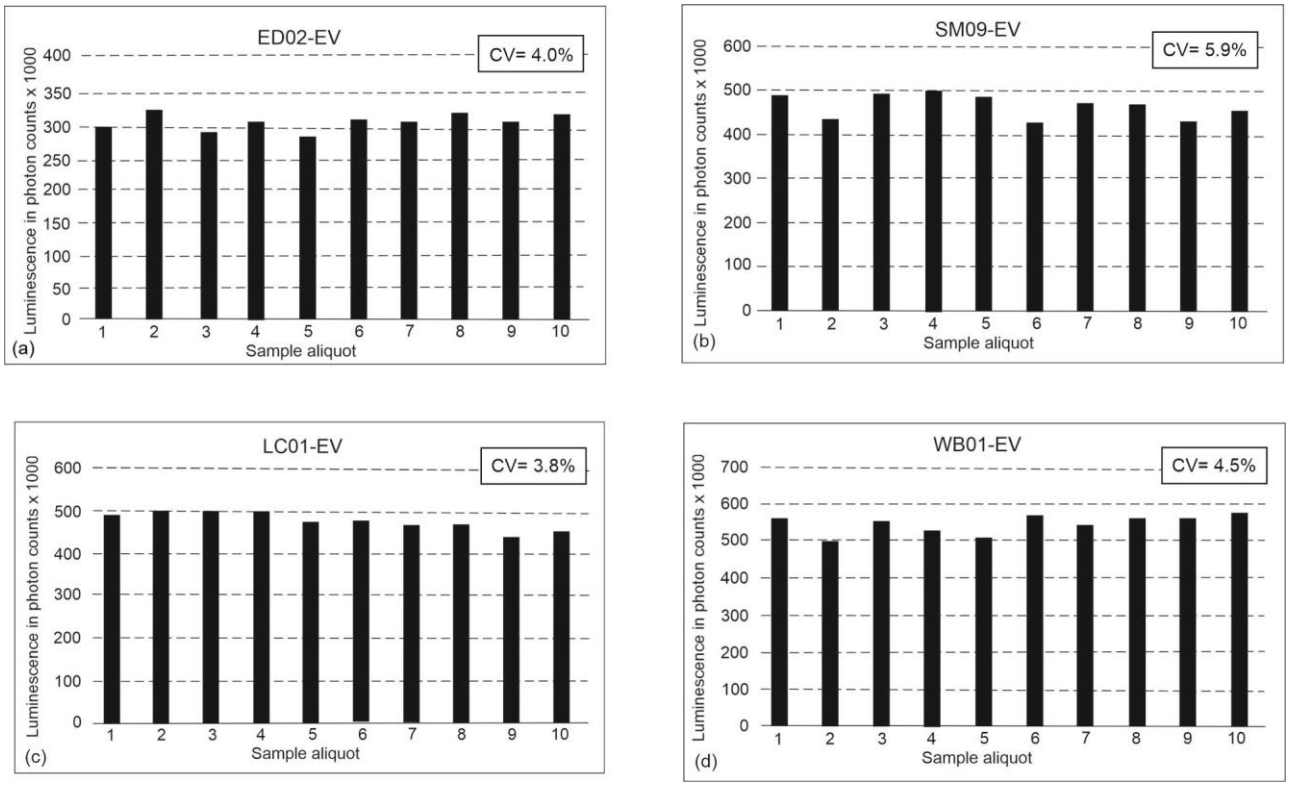

Fig. 6. *Ten selected signal intensities from aliquots prepared using equal-volume (EV) monogranular portions (~1.5 g) for each site. CV denotes the coefficient of variation calculated for the set.*

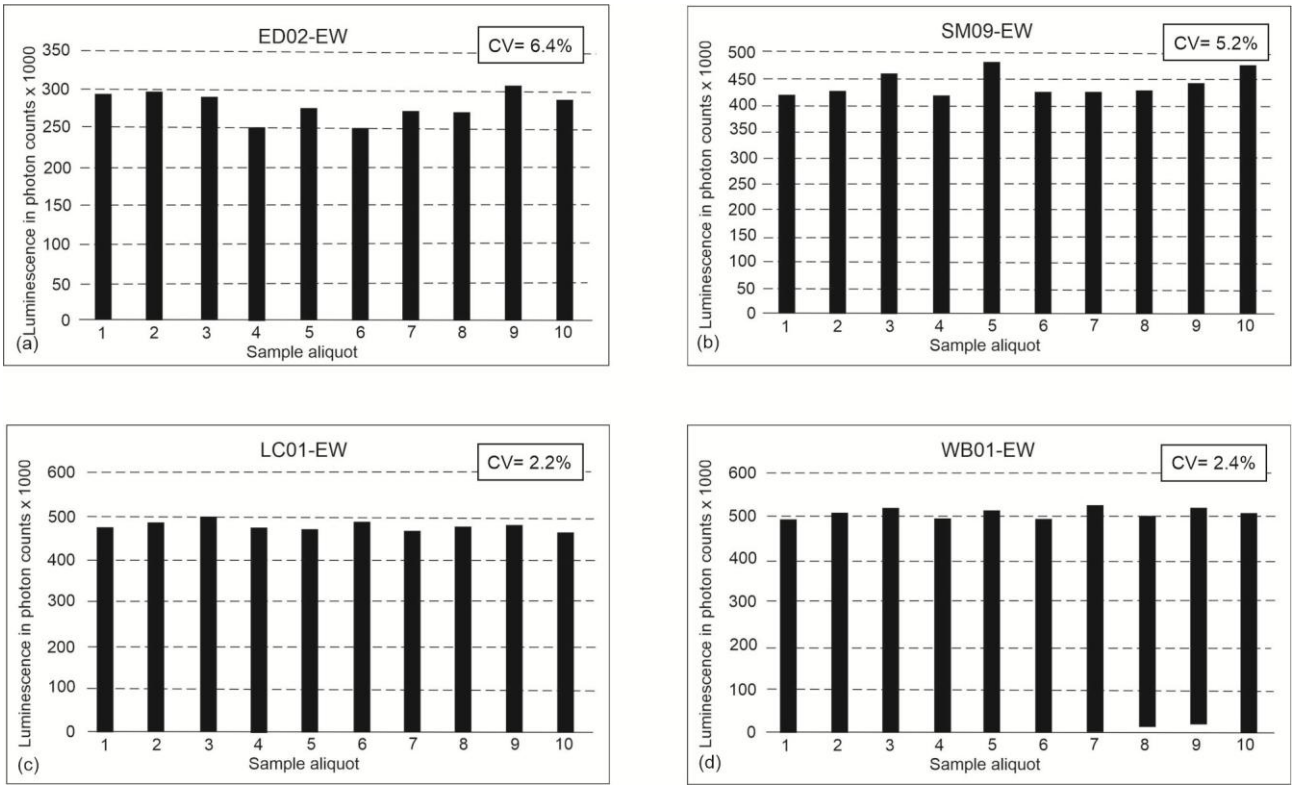

Fig. 7. *Ten selected signal intensities from aliquots prepared using equal-weight (EW) monogranular portions (1.5 g) for each site. CV denotes the coefficient of variation calculated for the set.*

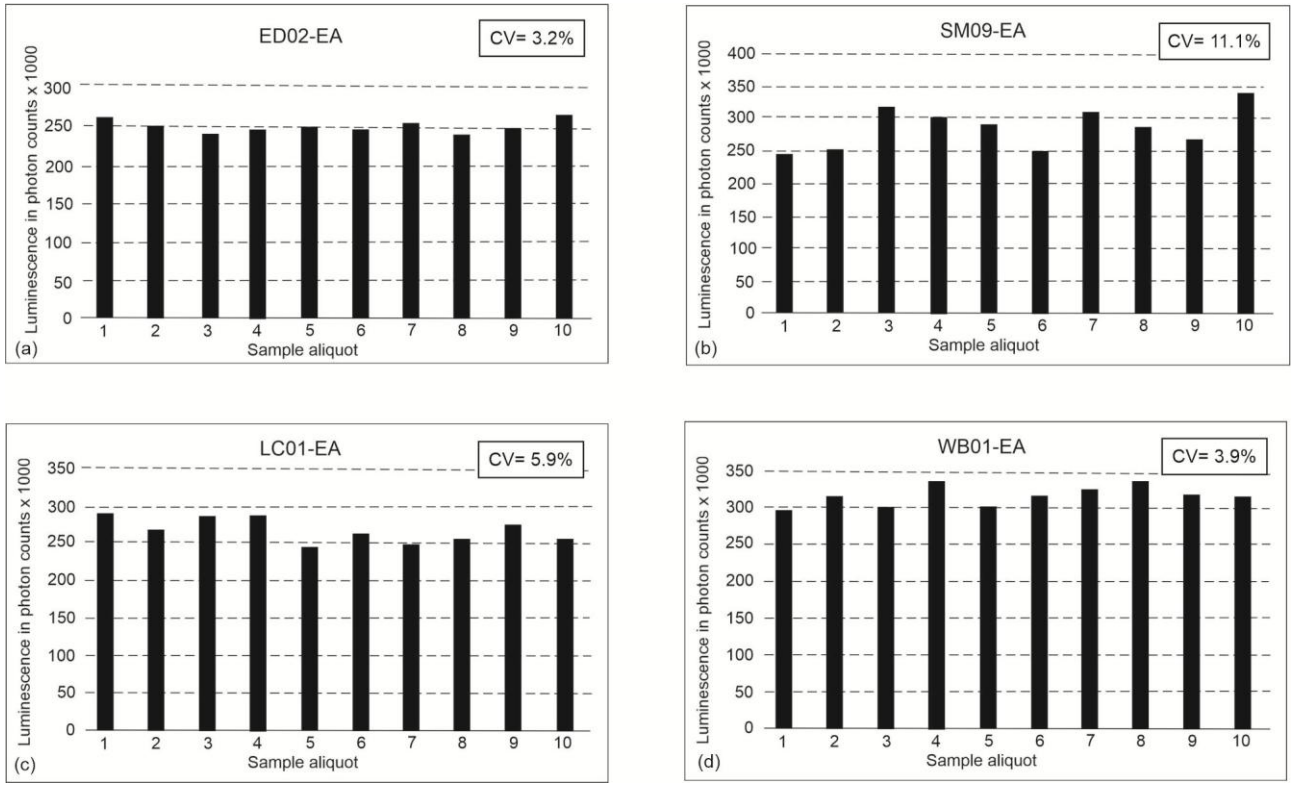

Fig. 8. *Ten selected signal intensities from aliquots prepared using equal-area (EA) monogranular portions (~1.0 g) affixed to adhesive tape segments for each site. CV denotes the coefficient of variation calculated for the set.*

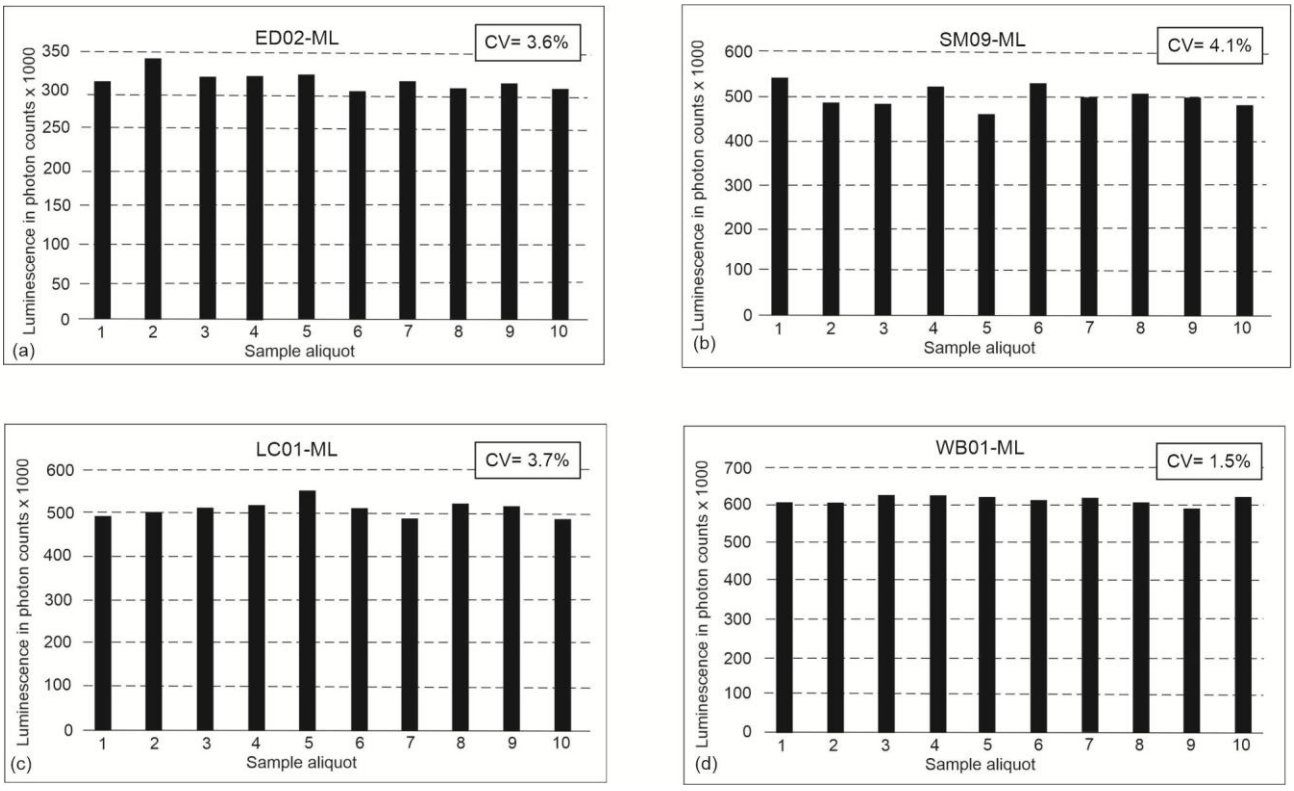

Fig. 9. *Ten selected signal intensities from aliquots prepared using equal-weight multilayer (ML) portions weighing 12.0 g for each site. CV denotes the coefficient of variation calculated for the set.*

3.3. IRSL signals from different aliquot preparation methods

To assess potential differences in mineralogical behaviour between quartz and feldspar, and contrast the reproducibility of their signals, the IRSL data in **Table 4** were evaluated using coefficients of variation (CV), following the same approach as for the blue-OSL data. Results are presented in **Table 6**. As with the blue-OSL data, reproducibility varied between samples: e.g. WB01 yielded tightly clustered IRSL signals (CV = 3.4–4.9%), whereas SM09 showed moderate to high variability (CV = 8.6–13.3%). The remaining samples (LC01 and ED02) exhibited low to moderate variability.

With respect to aliquot preparation methods, the CV values for IRSL data indicate that no single method consistently produced tightly clustered data across all sites. The equal-weight monolayer (EW), equal-area (EA), and equal-weight multilayer (ML) methods yielded consistent signals for two sites but not the others, while the equal-volume (EV) method produced tightly clustered IRSL data only for WB01.

3.4 Depletion indices and IRSL/OSL Ratios

Table 7 presents IRSL and blue-OSL depletion indices for each aliquot analyzed for sample ED02-EV. These were calculated as the ratio of total photon counts from the first 30 s of stimulation to those from the final 30 s. Signals associated with the most recent burial event typically deplete more rapidly than those inherited from earlier events due to partial bleaching (Sanderson and Murphy, 2010). Thus, the ratio provides an indicator of bleaching at burial. Depletion ratios for the remaining IRSL and blue-OSL measurements in **Table 4** are provided as supplementary data. Overall, depletion indices were relatively consistent across aliquots within each sample and across preparation methods, generally ranging from 1.200 to 1.355. This indicates dominance of rapidly depleting signals, characteristic of well-bleached sediments. Variations in mineralogical composition of aliquots can also influence depletion indices, but no such effect is evident in this case.

IRSL/OSL ratios were calculated for each aliquot measurement as shown for ED02-EV in **Table 7**. The rest of the calculations are provided as supplementary data. Overall, ratios for each set of ten aliquots are relatively consistent, indicating minimal variation in feldspar-to-quartz proportions between aliquots. To compare differences among preparation methods, mean IRSL/OSL ratios were calculated for each method (**Table 8**). Two trends are evident. First, there is a clear site dependence: samples from ED01, LC01, and WB01 show relatively similar ratios (0.4292–0.5095), whereas sample SM09 is consistently lower (0.3399–0.3990). This likely reflects a lower feldspar content in SM09 relative to the other sites, attributable to differences in sediment provenance.

Table 7. *Depletion indices and IRSL/OSL ratios for signals obtained from monogranular portions of equal volume for Sample ED02 (ED02-EV).*

#	IRSL	Depletion Index	Blue-OSL	Depletion Index	IRSL/OSL
1	136500 ± 370	1.280 ± 0.008	301147 ± 549	1.225 ± 0.004	0.514 ± 0.002
2	137482 ± 371	1.269 ± 0.008	318042 ± 564	1.252 ± 0.004	0.458 ± 0.002
3	130356 ± 362	1.251 ± 0.008	288286 ± 537	1.210 ± 0.004	0.487 ± 0.002
4	136467 ± 370	1.277 ± 0.008	304932 ± 553	1.200 ± 0.004	0.465 ± 0.002
5	130784 ± 362	1.270 ± 0.008	280874 ± 530	1.119 ± 0.004	0.428 ± 0.002
6	137742 ± 372	1.265 ± 0.008	309783 ± 557	1.228 ± 0.004	0.488 ± 0.002
7	156578 ± 396	1.302 ± 0.008	305111 ± 553	1.208 ± 0.004	0.456 ± 0.002
8	126099 ± 359	1.266 ± 0.006	317217 ± 564	1.232 ± 0.004	0.443 ± 0.002
9	135826 ± 369	1.260 ± 0.008	305214 ± 553	1.225 ± 0.004	0.460 ± 0.002
10	135888 ± 369	1.248 ± 0.008	315138 ± 562	1.210 ± 0.004	0.490 ± 0.002

 # - Aliquot sequence number; IRSL- infrared stimulated luminescence; Blue-OSL-blue optically stimulated luminescence; ED02-EV – Sample ED02 equal volume aliquots.

A second trend is that, for all four samples, aliquots prepared using double-sided adhesive tape consistently yield higher mean IRSL/OSL ratios (e.g., 0.5096 for ED02-EA) than those prepared using the other methods (e.g., 0.4507, 0.4651, and 0.4679 for ED02-EV, ED02-EW, and ED02-ML, respectively), by approximately 8–17%. Notably, adhesive-tape aliquots are the smallest (~1.0 g), raising the possibility that a small number of bright feldspar grains disproportionately influence the signal. However, this is not supported by the data, as aliquots prepared using other methods with intermediate masses (~1.5 g; ED02-EV and ED02-EW) yield IRSL/OSL ratios comparable to those from much larger aliquots (~12 g; ED02-ML). A more plausible explanation is that the adhesive tape preferentially retains feldspar grains relative to quartz, thereby increasing the feldspar contribution to the measured signal and elevating the IRSL/OSL ratio.

3.5. Grain size distribution

Grain size properties for the four samples calculated using the Folk and Ward (1957) method are provided in **Table 9**. Sample WB01 comprises very fine sand with a mean size of 99.5 μm. The other three samples all comprise fine sand with sizes ranging from 140.6 μm (ED02) to 149.6 μm (LC01) and 217.2 μm (SM09). All samples are moderately well sorted, apart from WB01 which is moderately sorted. Similarly, all samples are symmetrically skewed apart from WB01 which is fine skewed. Kurtosis is indicated in **Table 9**.

Table 8. *Mean IRSL/OSL values for each set of 10 aliquots from each aliquot preparation method.*

Site	**Edson**			
Mounting method	ED02-EV	ED02-EW	ED02-EA	ED02-ML
Mean IRSL/OSL	0.4507	0.4651	0.5095	0.4679
Site	**Smith**			
Mounting method	SM09-EV	SM09-EW	SM09-EA	SM09-ML
Mean IRSL/OSL	0.3399	0.3573	0.3980	0.3620
Site	**La Crete**			
Mounting method	LC01-EV	LC01-EW	LC01-EA	LC01-ML
Mean IRSL/OSL	0.4432	0.4358	0.5009	0.4292
Site	**Wood Buffalo**			
Mounting method	WB01-EV	WB01-EW	WB01-EA	WB01-ML
Mean IRSL/OSL	0.4558	0.4439	0.5030	0.4414

EV- Equal-volume monogranular layer aliquot; EW- Equal-weight monogranular layer aliquot; EA- Equal-area monogranular layer aliquot mounted on adhesive tape; ML-Equal-weight multilayer aliquot.

Table 9. *Grain size distribution.*

Measure	**Sample**			
	ED02	**SM09**	**LC01**	**WB01**
Mean	140.6 μm (fine sand)	217.2 μm (fine sand)	149.6 μm (fine sand)	99.49 μm (very fine sand)
Sorting	1.490 (moderately well sorted)	1.541 (moderately well sorted)	1.615 (moderately well sorted)	1.825 (moderately sorted)
Skewness	0.002 (symmetrical)	0.030 (symmetrical)	0.014 (symmetrical)	-0.106 (fine skewed)
Kurtosis	1.004 (mesokurtic)	0.976 (mesokurtic)	1.011 (mesokurtic)	2.117 (Very leptokurtic)

4. Discussion

4.1 Influence of aliquot geometry and size on blue-OSL signal consistency

The evaluation of optimal aliquot preparation strategies for portable OSL readers necessitates a thorough understanding of the interplay between sample size, geometry, and the resulting luminescence signal. The variation of the signal intensity with sample size depicted in **Fig. 4** shows that for both IRSL and blue-OSL the signal increased rapidly as the surface area of the sample aliquot increased. This is because, in continuous-wave mode, the portable OSL reader measures the cumulative luminescence signal, which is the sum of photon contributions from all luminescent grains in a given aliquot. Hence, larger aliquot surface areas, which expose greater numbers of sediment grains to the stimulating source, consistently yield higher luminescence signals, underscoring the influence of sample geometry on signal intensity. The sharp increase in signal intensity with surface area highlights a fundamental requirement for preparing reproducible aliquots: ensuring that each aliquot is mounted with equal surface area. Standardizing this parameter is therefore critical for minimizing variability and establishing reliable comparisons in portable OSL studies. In theory, the most straightforward way to ensure equal and reproducible surface area is to cover the entire base of the Petri dish.

Fig. 4 also shows that once the base of the Petri dish is fully covered, further increases in sample weight that result from additional grain layers above the bottom layer lead to continued signal growth for both IRSL and blue-OSL, though at a lower rate than during the initial surface area increase. This clearly indicates that the stimulating optical source penetrates the sediment column sufficiently to elicit measurable emissions. Notably, the rate of signal increase with thickness is lower than that observed with increasing surface area. A possible explanation is that sediment grains below the top layer are only partially exposed to the stimulating source, resulting in attenuation of the signal. Additionally, emissions from subsurface grains are partially scattered by the overlying layers, making them weaker than if the grains were exposed at the surface. Nonetheless, the increase in signal intensity with aliquot thickness highlights the importance of maintaining a constant thickness to improve measurement consistency.

Considering the above, the four aliquot preparation methods evaluated in this study can be classified into two main categories: monogranular layers and multilayer aliquots. Three of the methods tested fall into the monogranular layer category and the first of these was the approach that used a scoop to measure out aliquots of equal volume weighing about 1.5 g. The advantage of this approach as that it was the simplest and quickest method of preparing aliquots. However, a potential limitation was that, despite efforts to standardize aliquot volume, small variations in weight between scoops were observed. Hence, because the results in **Fig. 4** indicate that the signal varies with weight, some scatter is expected due to uncertainty in volume measurements. Nonetheless, results for three of the samples showed that the coefficient of variation (CV) that was obtained from the blue-OSL signal fell within the highly reproducible category. For the one sample that produced signals that were not highly reproducible, the values were marginally outside the highly clustered range with a CV of 5.9% (**Table 5**). Hence, overall, these results suggest that if the primary objective is speed of analysis rather than accuracy, this approach may be sufficient.

In the second monogranular layer method, aliquots of exactly 1.5 g were prepared to cover the base of the Petri dish. This method ensured the sample size in each aliquot was more consistent than in the volume method. However, the drawback of this method is that weighing out the exact amount is time-consuming, making it less attractive when speed is a priority. Despite the greater effort required to weigh aliquot portions accurately, the results were not very different from those obtained using the constant-volume method. The CV values for two of the samples indicated very tightly clustered measurements, while the other two were moderately consistent, with one falling just outside the highly reproducible range (**Table 5**).

In the first two monogranular methods, the aliquot preparation approach produced samples in which the sand grains were not fixed to the Petri dish. Hence, at least in theory, the grains may shift during transfer of the Petri dish into the OSL reader. It is also possible that, although the layer is mostly monogranular, some grains may sit atop one another. Consequently, these scenarios can cause signal variations between aliquots, even when the sample weight is identical. The third monogranular method addresses this problem by mounting sediment grains on adhesive tape affixed to equal-area cardstock segments that fit into the Petri dish. Using this method, two samples exhibited CV values indicative of highly reproducible blue-OSL signals, the third fell within the moderately reproducible range, while the fourth showed low consistency. These results were surprising as the method was expected to yield highly clustered data. However, possible reasons for the scatter include the small sample size (low number of grains) of about 1.0 g. Furthermore, it became evident that the number of grains retained by the adhesive tape during mounting depended on the level of pressure applied to the surface during mounting and it was not possible to ensure that this pressure was consistent on all aliquots. Thus, the number of grains retained by the adhesive tape varied between aliquots.

The final aliquot preparation method involved equal-weight sample portions (12 g), that produced aliquots approximately 3.5 mm thick in the Petri dish. All 4 samples yielded CV values of less than 5% (**Table 5**), suggesting that for these samples, this was a more reliable method of preparing aliquots with reproducible blue-OSL signals. Several factors may explain why these aliquots, significantly larger than the monogranular ones, yielded more consistent results, including:

a. Smaller samples contain fewer sediment grains. The total cumulative signal measured with the luminescence reader is a contribution from many grains. The more grains there are, the more representative the average is for any population of grains. Luminescence sensitivity also varies between grains. Thus, overall, larger samples are less susceptible to statistical noise (e.g. Duller, 2008).

b. Bulk samples, can contain multiple grain types including quartz and feldspar. Also, because feldspar grains can have a blue-sensitive dose that is not exhausted by the IRSL stimulation that is run prior to the blue-OSL, that heterogeneity between grains in a given sample is more pronounced in smaller samples than in large samples, which accentuates scatter in smaller samples.

c. Though this was not the case in this instance, in cases where the signals are much lower, the signal-to-noise ratio deteriorates for the smaller samples such that the noise becomes more substantial relative to the signal and the variability is accentuated.

d. Sample geometry and packing also come into play with smaller samples. A monolayer is much easier to disrupt when moving the sample such that the stimulation and signal detection become uneven. With multiple layers, however, it is easier to maintain a uniform surface layer as the movement of a few surface grains will simply result in the exposure of similar grains underneath.

Hence, overall, the observations in this study are consistent with the theory that larger samples are more likely to produce signals that are more consistent. The only drawback of this fourth method, as with the second method, is the need to weigh out precise sample portions, which can be time-consuming. Nonetheless, if the objective is rapid measurement, large equal-volume portions could be prepared, as in the first method, rather than weighing portions accurately.

It is also notable that apart from the variation of signals with the aliquot preparation method, there were some variations in reproducibility between samples, with some samples consistently yielding highly clustered signals irrespective of the preparation method (e.g. WB01), while others produced moderate and low consistency signals in most cases (SM09). Possible explanations for such variations include intrinsic sediment properties such as grain size, sorting, mineralogy, and sediment provenance. Sample WB01, for instance, comprises very fine sand which may have been very well bleached during eolian transport compared to the larger grain sizes noted in sample SM09.

Importantly, the samples analyzed in this study consist of moderately to well-sorted aeolian dune sands that were likely well bleached prior to burial. The sediments are easier to homogenize during aliquot preparation and have relatively simple mineralogy, being dominated by quartz with minor feldspar. Consequently, the findings of this study may not be universally applicable. Poorly sorted sediments with more variable mineralogical compositions are likely to exhibit different behaviour.

4.2 Influence of aliquot geometry and size on IRSL signal consistency

Aliquot geometry and size did not exhibit a consistent influence on the reproducibility of IRSL data in this study. Instead, sample site exerted a stronger control, with some samples yielding consistently reproducible signals, while others showed greater variability. This more complex behaviour compared to blue OSL signals likely reflects the properties of feldspar, which is subject to anomalous fading, the time-dependent loss of trapped charge at ambient temperatures after burial. Individual feldspar grains possess different defect structures and trap configurations, resulting in variable fading rates both within and between grains. In addition, different feldspar types (e.g. K-feldspar and Na-rich feldspar) can exhibit distinct fading behaviours (Huntley and Lamothe, 2001; Kars *et al.*, 2008).

In conventional luminescence dating, fading rates must be measured and corrected for. However, this is beyond the scope of this study, and the overall impact of fading on aliquot reproducibility is difficult to quantify. Thus, it is not possible to definitively determine from this study why IRSL signals behave differently from blue OSL signals, particularly in not producing greater inter-aliquot consistency with increasing aliquot size. Repeating the study using samples in which feldspar is more abundant relative to quartz may provide further insight into this discrepancy.

4.3. Effects of variations in mineralogy and other sediment properties on signal reproducibility

As discussed above, sediment pretreatment, such as sieving to obtain narrower grain-size fractions and removing carbonates and luminescent heavy minerals, has been shown to reduce portable luminescence signal scatter in some cases (e.g., Gray *et al.*, 2018). In this study, however, the dune sands comprise predominantly quartz, with feldspars forming a smaller component. Hence, no other major luminescence contributors occur in the samples, apart from quartz and feldspar.

The IRSL/OSL ratio was highly consistent between aliquots within each sample and showed little variation between samples from different sites. This indicates that inter-aliquot variation in feldspar-to-quartz proportions was minimal and not likely a significant contributor to variability compared to aliquot size and sample geometry. Similarly, depletion indices for both IRSL and blue-OSL signals were consistent across samples and aliquot preparation methods, suggesting that both feldspar and quartz grains were well bleached prior to burial.

Overall, these results are consistent with the inference that sample geometry and aliquot size exerted the dominant control on inter-aliquot reproducibility of blue-OSL data in this study. In contrast to the blue-OSL data, however, IRSL signals were more strongly influenced by the sample site of origin.

5. Conclusions

Portable OSL measurements offer an efficient means of obtaining sub-stratigraphic information in geoscience and archeological field sciences. However, the utility of the measurements depends on the reproducibility of the signals they generate. Establishing consistent measurement protocols, including sample aliquot preparation, is therefore essential if these signals are to be used as reliable proxies for geomorphic processes. The investigation of the variation of luminescence signal intensities with sample size as well as an evaluation of sample preparation strategies conducted with a portable OSL reader in this study have shown that:

- The luminescence signal yielded by a sample aliquot varies with the surface area of the sample exposed to the stimulating source. The relationship between sample size and signal intensity appears to be sublinear. Consequently, normalizing signals by sample weight may introduce bias unless the underlying scaling relationship between signal and sample size is first quantified.
- The signal also increases with sample thickness, though at a slower rate compared to increases in surface area.
- To optimize consistency in portable OSL aliquot preparation, it is important to control both the surface area and the thickness of the sample. Preparing aliquots with a fixed surface area ensures that a comparable number of grains are directly exposed to the stimulating light, while maintaining uniform thickness minimizes variability in the contribution from grains at different depths. Together, these controls enhance reproducibility and allow for more reliable comparison of luminescence signals across aliquots.
- Aliquots containing larger sample portions tend to produce blue-OSL signals with lower variability than those derived from smaller samples. As a result, multilayer aliquots are more likely to yield tightly clustered blue-OSL signals compared to monogranular preparations.
- Aliquots made by weighing out fixed-weight portions were shown to yield the best results for blue-OSL signals. However, portions created using a fixed volume were also shown to give highly consistent results for some samples, in addition to the fact that preparing aliquots using a fixed volume can be done more rapidly than by weight. Hence, in contexts where speed of analysis is prioritized over accuracy, aliquots for blue-OSL analysis could be prepared using a fixed-volume measuring device as opposed to measuring by weight.
- Inter-aliquot reproducibility of IRSL signals was more strongly controlled by sample site than by aliquot size or geometry.

This study employed eolian sediments comprising mostly fine sand with minimal silt fractions. Hence, it was easy to mix them thoroughly to ensure the samples were homogenous prior to measuring with the portable OSL reader. Poorly sorted sediments with complex mineralogy are likely to exhibit more complex behaviour than those analyzed in this study. Future work should consider a broader range of sediment types, including loess, fluvial sediments, soils, and colluvial materials, for which portable OSL readers are commonly applied.

Supplementary Data

Supplementary material comprising luminescence data collected in this study can be found online at https://doi.org/10.20858/geochr/220626

Acknowledgements

The author would like to thank Harrison Gray and an anonymous reviewer for the constructive feedback provided during the review process. Susan Fryters is thanked for reading earlier versions of the manuscript.

References

Adolph ML, Lampe R, Lorenz S and Haberzettl T, 2021. Characterization of (paleo)lacustrine landforms using sedimentological and portable OSL investigations at Schweriner See, north-eastern Germany. *Earth Surface Processes and Landforms* 47(2): 422–435, DOI 10.1002/esp.5258.

Bateman MD, Stein S, Ashurst RA and Selby K, 2015. Instant luminescence chronologies? High resolution luminescence profiles using a portable luminescence reader. *Quaternary Geochronology* 30: 141–146, DOI 10.1016/j.quageo.2014.12.007.

Ben-Melech N, Zeevi-Berger O, Porat N, Roskin J, Langgut D, Walker B and Gadot Y, 2024. Agricultural terracing and land tenure in Late Medieval Southern Levant: The Case of Nahal Ein Karim, Jerusalem. *Environmental Archaeology* 1–15, DOI 10.1080/14614103.2024.2371052.

Boyd SL, Kinnaird TC, Srivastava A, Whittaker JE and Bates CR, 2022. Investigation of coastal environmental change at Ruddons Point, Fife, S.E. Scotland. *Scottish Journal of Geology* 58: sjg2022-005, DOI 10.1144/sjg2022-005.

Blott SJ and Pye K, 2001. GRADISTAT: A grain size distribution and statistics package for the analysis of unconsolidated sediments. *Earth Surface Processes and Landforms* 26: 1237–1248, DOI 101002/esp.261.

Dalton AS, Dulfer HE, Margold M, Heyman J, Clague JJ, Froese DG, Gauthier MS, Hughes ALC, Jennings CE, Norris, SL and Stoker BJ, 2023. Deglaciation of the North American Ice sheet complex in calendar years based on a comprehensive database of chronological data: NADI-1. *Quaternary Science Reviews* 321: 108345, DOI 10.1016/j.quascirev.2023.108345.

Duller GAT, 2008. Single-grain optical dating of Quaternary sediments: why aliquot size matters in luminescence dating. *Boreas* 37(4): 589–612, DOI 10.1111/j.1502-3885.2008.00051.x.

DuRoss CB, Gold RD, Gray HJ, and Nicovich SR, 2022. Portable optically stimulated luminescence age map of a paleoseismic exposure. *Geology 50*(4): 470–475, DOI 10.1130/G49472.1.

Dyke AS, Andrews JT, Clark PU, England JH, Miller, GH, Shaw J and Veillete JJ, 2002. The Laurentide and Inuitian ice sheets during the Last Glacial Maximum. *Quaternary Science Reviews* 21: 9–31, DOI 10.1016/S0277-3791(01)00095-6.

Euzen C, Chabaux F, Rixhon G, Preusser F, Eyrolle F, Chardon V, Zander AM, Badariotti D and Schmitt L, 2024. Multi-method geochronological approach to reconstruct post-1800 floodplain sedimentation in the upper Rhine plain, France. *Quaternary Geochronology* 83: 101561, DOI 10.1016/j.quageo.2024.101561.

Folk RL and Ward WC, 1957. Brazos river bar: a study in the significance of grain size parameters. *Journal of Sedimentary Petrology* 27: 3–26, DOI 10.1306/74D70646-2B21-11D7-8648000102C1865D.

Fu RR, Weiss BP, Lima EA, Kehayias P, Araujo JFDF, Glenn DR, Gelb J, Einsle JF, Bauer AM, Harrison RJ, Ali GAH and Walsworth RL, 2017. Evaluating the paleomagnetic potential of single zircon crystals using the Bishop Tuff. *Earth and Planetary Science Letters* 458: 1–13, DOI 10.1016/j.epsl.2016.09.038.

Gray HJ, Mahan SA, Springer KB, and Pigati JS, 2018. Examining the relationship between portable luminescence reader measurements and depositional ages of paleowetland sediments, Las Vegas Valley, Nevada. *Quaternary Geochronology* 48: 80–90. DOI 10.1016/j.quageo.2018.07.006.

Gray H, DuRoss C, Nicovich S and Gold R, 2022. Luminescence sediment tracing reveals the complex dynamics of colluvial wedge formation. *Science Advances* 8(22): eabo0747, DOI 10.1126/sciadv.abo0747.

Holter ME, 1971. Silica (dune) sand from the Medicine Hat area, Alberta; Research Council of Alberta, *RCA/AGS Earth Sciences Report* 1971-05, 25 p.

Huntley DJ and Lamothe M, 2001. Ubiquity of anomalous fading in K-feldspars and the measurement and correction for it in optical dating Available to Purchase. Canadian Journal of Earth Sciences 38 (7): 1093–1106, DOI 10.1139/e01-013.

Kars RH, Wallinga J and Cohen KM, 2008. A new approach towards anomalous fading correction for feldspar IRSL dating — tests on samples in field saturation. Radiation Measurements 43, 786–790. DOI 10.1016/j.radmeas.2008.01.021.

Kinniard T, Bolos J, Turner A and Turner S, 2017. Optically-stimulated luminescence profiling and dating of historic agricultural terraces in Catalonia (Spain). *Journal of Archaeological Science* 78: 77–77, DOI 10.1016/j.jas.2016.11.003.

Kinnaird T, Dawson T, Sanderson D, Hamilton D, Cresswell A and Rennell R, 2019. Chronostratigraphy of an eroding complex Atlantic roundhouse, Baile Sear, Scotland. *Journal of Island and Coastal Archaeology* 14(1): 46–60, DOI 10.1080/15564894.2017.1368744.

Majgier R., Maternicki, K, Mandowski A, Moska P, Biernacka M and Kreutzer S, 2025. The Helios OSL reader: a portable system for dating and dosimetry applications. *Geochronometria* 52: 208873, DOI 10.20858/geochr/208873.

Muños-Salinas E, Castillo M, Arce JL, Correa-Metrio A, Cruz-Zaragoza E and Valoix A, 2023. Using fallout ^{137}Cs and OSL as sediment tracers in badlands: a case study of Tepezalá volcano (Central Mexico). Geografiska Annaler: Series A, Physical Geography 105(1): 27–46, DOI 10.1080/04353676.2023.2171999.

Munyikwa K and Brown S, 2014. Rapid equivalent dose estimation for eolian dune sands using a portable OSL reader and polymineralic standardised luminescence growth curves: Expedited sample screening for OSL dating. *Quaternary Geochronology* 22: 116–125, DOI 10.1016/j.quageo.2014.04.002.

Munyikwa K, Kinnaird TC and Sanderson DCW, 2021. The potential of portable luminescence readers in geomorphological investigations: a review. *Earth Surface Processes and Landforms* 46: 131–150, DOI 10.1002/esp.4975.

Munyikwa K, Rittenour T and Feathers J, 2017. Temporal constraints for the Late Wisconsinan deglaciation of western Canada using eolian dune chronologies from western Canada. *Palaeogeography, Palaeoclimatology, Palaeoecology* 470: 147–165, DOI 10.1016/j.palaeo.2016.12.034.

Nitundil S, Stone A and Srivasatava A, 2023. Applicability of using portable luminescence reader for rapid age-assessment of dune accumulation in the That desert, India. *Quaternary Geochronology* 78: 101468, DOI 10.1016/j.quageo.2023.101468.

Porat N, Lopez GI, Lensky N, Elinson R, Avni Y, Elgart-Sharon Y, Faershtein G and Gadot Y, 2019. Using portable OSL reader to obtain a time scale for soil accumulation and erosion in archaeological terraces, the Judean Highlands, Israel. *Quaternary Geochronology* 49: 65–70, DOI 10.1016/j.quageo.2018.04.001.

Portenga EW and Bishop P, 2016. Confirming geomorphological interpretations based on portable OSL reader data. *Earth Surface Processes and Landforms* 41(3): 427–432, DOI 10.1002/esp.3834.

Rex CL, Staff RA, Sanswerson DCW, Cresswell AJ, Marshall MH, Hyodo M, Horiuchi D, Tada R and Nagakawa T, 2022. Controls on luminescence signals in lake sediment cores. A study from Lake Suigetsu, Japan. *Quaternary Geochronology* 71(5): 101319, DOI 10.1016/j.quageo.2022.101319.

Rizza M, Rixhon G, Valla PG, Gairoard S, Delanghe D, Fleury J, Tal M and Groleau S, 2024. Revisiting a proof of concept in quartz-OSL bleaching processes using sands from a modern-day river (the Séveraisse, French Alps). *Quaternary Geochronology* 82(1): 101520, DOI 10.1016/j.quageo.2024.101520.

Robins L, Roskin J, Marder O, Edeltin, L, Yu L and Greenbaum N, 2023. Geomorphic, environmental and archeological significance of Last Glacial Maximum to middle Holocene dune damming, northwestern Negev dunefield margin, Israel. *Quaternary Science Reviews* 308: 108098, DOI 10.1016/j.quascirev.2023.108098.

Robins L, Roskin J, Yu L, Bookman R and Greenbaum N, 2022. Aeolian-fluvial processes control landscape evolution along dunefield margins of the north-western Negev (Israel) since the Late Quaternary. *Quaternary Science Reviews* 285: 107520, DOI 10.1016/j.quascirev.2022.107520.

Roman M, Píšková A, Sanderson DCW, Cresswell AJ, Bulínová M, Pokorný M, Kavan J, Jennings SJA, Lirio JM, Nedbalová L, Sacherová V, Kopalová, K, Glasser NF and Nývlt D, 2024. The Late Holocene deglaciation of James Ross Island, Antarctic Peninsula: OSL and C14 dated multi-proxy sedimentary record from Monolith Lake. *Quaternary Science Reviews* 33: 108863, DOI 10.1016/j.quascirev.2024.108693.

Sánchez-Pardo JC, Silva-Sánchez N, Kinnaird T, Turner S, Brandolini F, Carrer F, Srivastava A, López-Salas E and Vilariño O, 2024. Dating and characterizing the transformation of a Monastic landscape. A Multidisciplinary approach to the agrarian spaces of Samos Abbey (NW Spain). *Environmental Archaeology* 31: 81–99, DOI 10.1080/14614103.2024.2319954.

Sanderson DCW and Murphy S, 2010. Using simple portable measurements and laboratory characterisation to help understand complex and heterogeneous sediment sequences for luminescence dating. *Quaternary Geochronology* 5: 299–305, DOI 10.1016/j.quageo.2009.02.001.

Schulze T, Schwahn L, Fülling A, Zeeden C, Preusser F and Sprafke T, 2022. Investigating the loess-palaeosol sequence of Bahlingen-Schonenberg (Kaiserstuhl), southwestern Germany, using a multi-methodological approach. *E&G Quaternary Science Journal* 71: 145–162, DOI 10.24451/arbor.21443.

Srivastava A, Kinniard T, Sevara C, Holcomb JA and Turner S, 2023. Dating agricultural terraces in the Mediterranean using luminescence: Recent progress and challenges. *Land* 12 (3): 716, DOI 10.3390/land12030716.

Staff RA, Sanderson DCW, Rex CL, Cresswell A, Hyodo M, Kitaba I, Marshall MH, Schlolaut G, Yamada K, Suzuki Y, Nowinski V, Tada R and Nakagawa T, 2024. A luminescence-derived cryptostratigraphy from the Lake Suigetsu sedimentary profile, Japan: 45,000–30,200

IntCal20 yr BP. *Quaternary Geochronology* 83: 101588, DOI 10.1016/j.quageo.2024.101588.

Stone A, Bateman MD, Burrough SL, Garzanti E, Limonta M, Radeff G and Telfer MW, 2019. Using a portable luminescence reader for rapid age assessment of aeolian sediment for reconstructing dunefield landscape evolution in southern Africa. *Quaternary Geochronology* 49: 57–64, DOI 10.1016/j.quageo.2018.03.002.

Stone A, Bateman MD, Sanderson D, Burrough SL, Cutt R and Cresswell A, 2024. Probing sediment burial age, provenance, and geomorphic processes in dryland dunes and lake shorelines using portable luminescence data. *Quaternary Geochronology* 82: 101542, DOI 10.1016/j.quageo.2024.101542.

Stone AEC, Bateman MD and Thomas DSG, 2015. Rapid age assessment in the Namib Sand Sea using a portable luminescence reader. *Quaternary Geochronology* 30: 134–140, DOI 10.1016/j.quageo.2015.02.002.

Timar-Gabor A, Buylaert JP, Guralnik B, Trandafir-Antohi O, Constantin D, Anechitei-Deacu V, Jain M, Murray AS, Porat N, Hao Q and Wintle AG, 2017. On the importance of grain size in luminescence dating using quartz. *Radiation Measurements* 106: 464–471, DOI 10.1016/j.radmeas.2017.01.009.

Wolfe SA, Huntley DJ and Ollerhead J, 2004. Relict Late Wisconsinan dune fields of the Northern Great Plains, Canada. *Géographie physique et Quaternaire* 56: 203–214, DOI 10.7202/013146ar.